iScience, Volume *26*

Supplemental information

Energy transfer and trapping in photosystem I with and without chlorophyll-*f*

Ivo H.M. van Stokkum, Marc G. Müller, Jörn Weißenborn, Sebastian Weigand, Joris J. Snellenburg, and Alfred R. Holzwarth

Contents

Fit quality of the Global Analysis of the transient absorption dynamics in reduced PSI of SCy6803

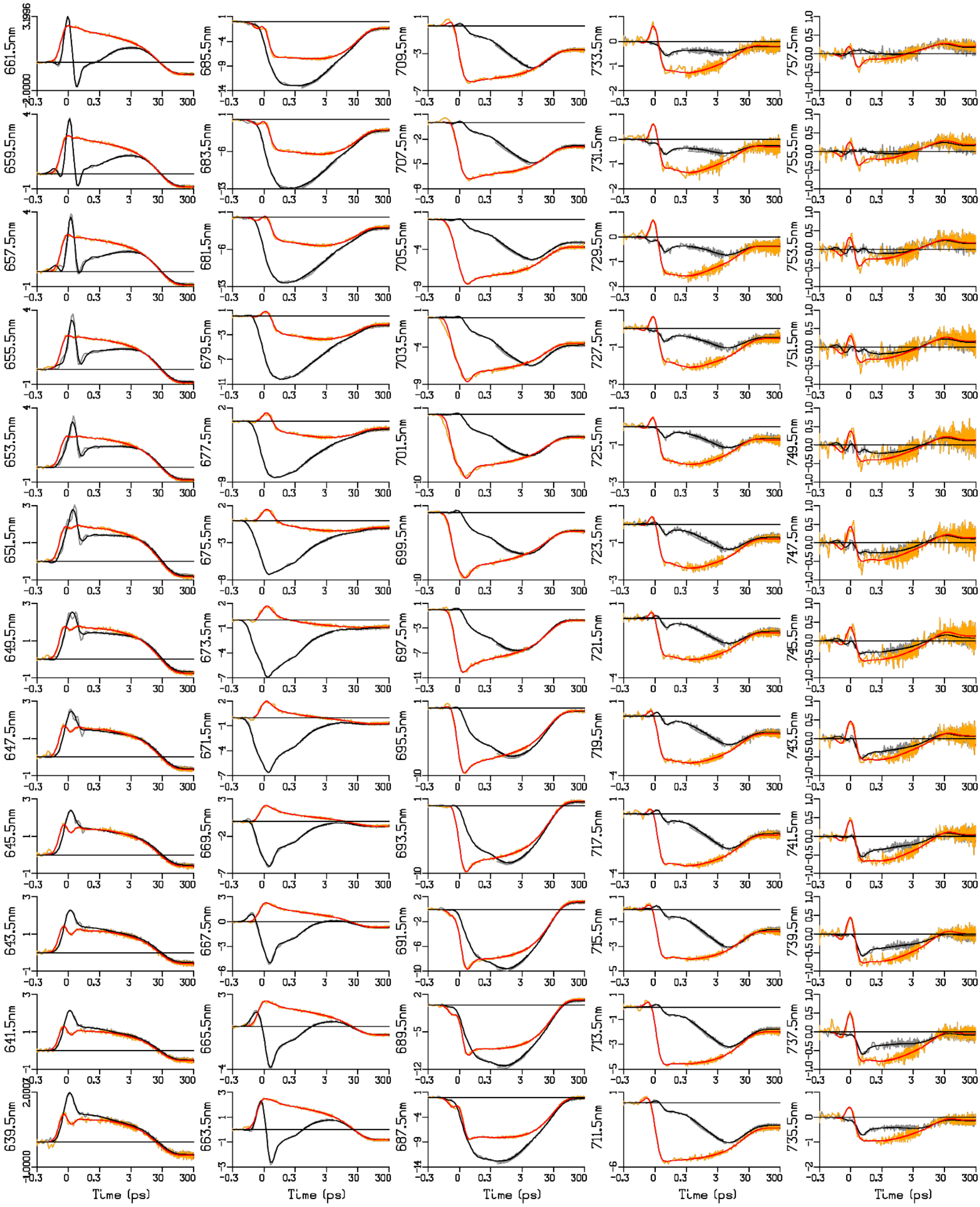

Figure S 1. Transient absorption (in units of mOD) of SCy6803 WL-PSI in the reduced form at 60 selected wavelengths (indicated in the ordinate label) (related to Figure 3). Key: 670 nm excitation (grey), 700 nm excitation (orange). Black and red lines indicate the global analysis fit. Note that the time axis is linear until 0.3 ps and logarithmic thereafter. Note also that each panel is scaled to its maximum. The overall rms error of the fit was 0.067 mOD.

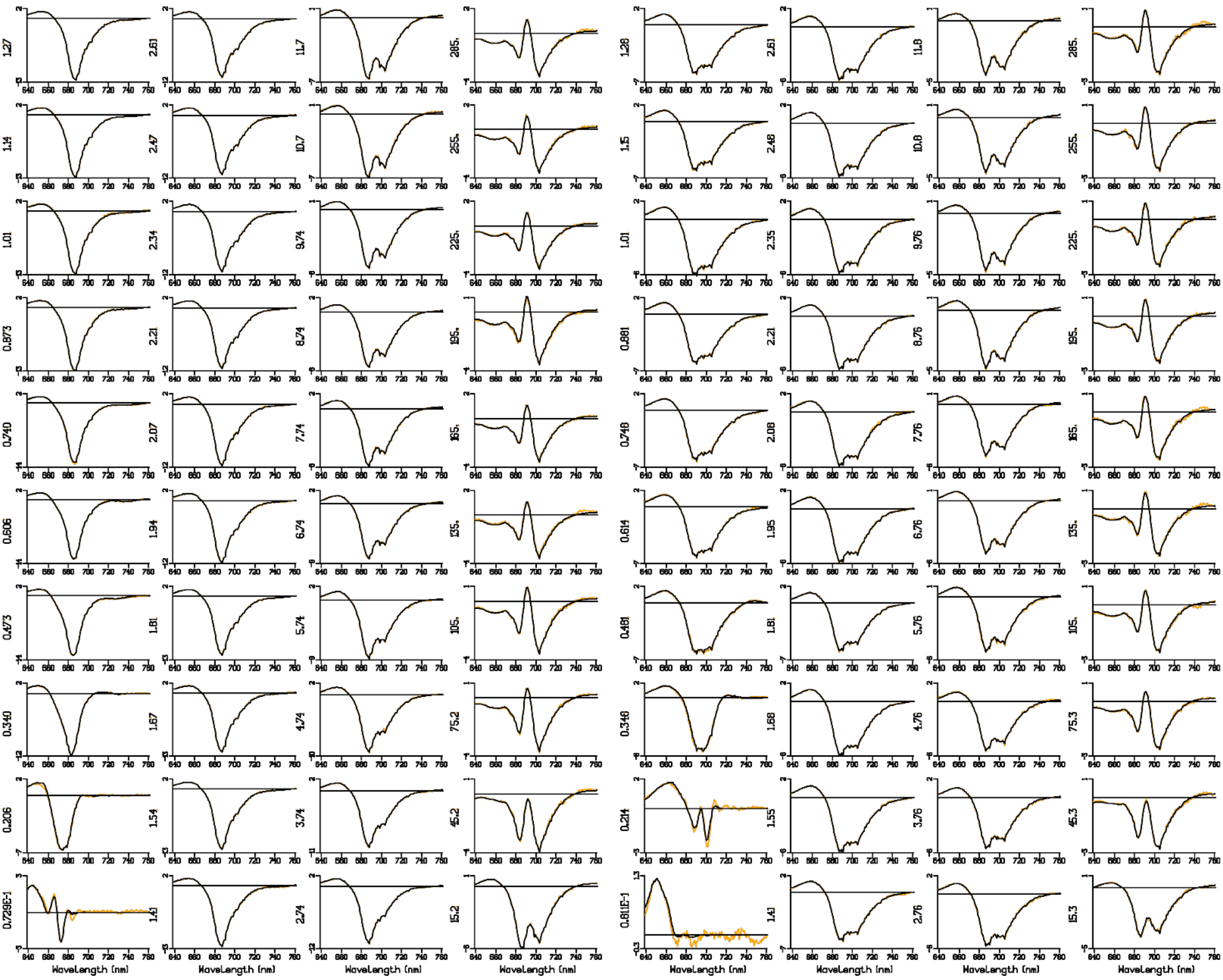

Figure S 2. Transient absorption (in units of mOD) of SCy6803 WL-PSI in the reduced form at forty selected time delays (indicated in the ordinate label, in ps) (related to Figure 3). Left four columns, 670 nm excitation; right four columns, 700 nm excitation. Key: data (orange). Black lines indicate the global analysis fit. The overall rms error of the fit was 0.067 mOD. The dispersion (of 0.4 ps over the whole wavelength range) is clearly visible as the early detection (around 0.08 ps) of the signal (black) around 650 nm.

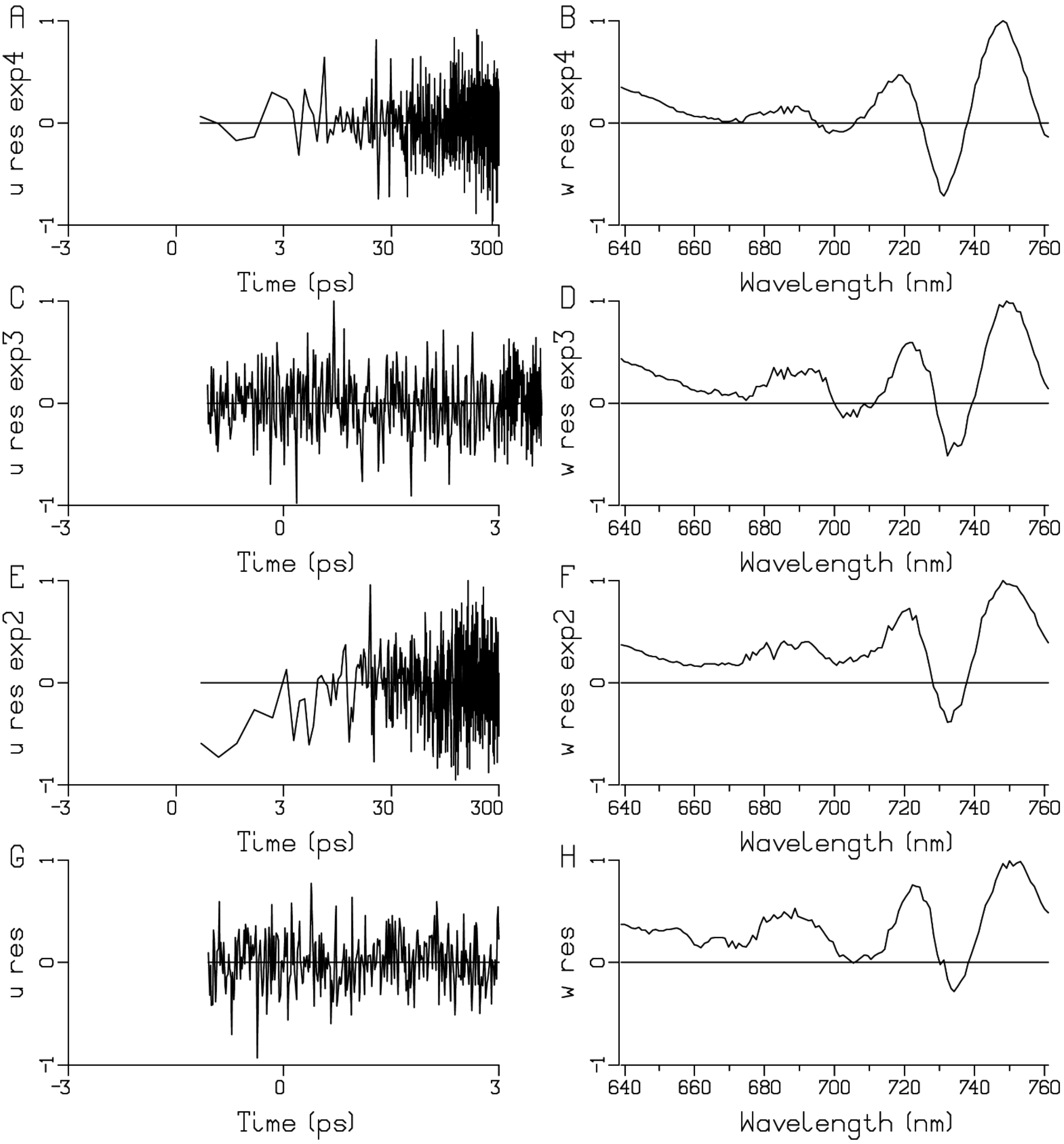

Figure S 3. First left (A,C,E,G) and right (B,D,F,H) singular vectors resulting from the singular value decomposition (SVD) of the residual matrix of WL-PSI of WT Synechocystis PCC6803 resulting from the *global* analysis (related to Figure 3). Note that all first left singular vector panels (A,C,E,G) show no trends at all. Key A,B: WL 700 nm excitation TimeRange(TR)2; C,D: WL 700 nm excitation TR1; E,F: WL 670 nm excitation TR2; G,H: WL 670 nm excitation TR1. Note that the time axis in (A,C,E,G) is linear until 3 ps and logarithmic thereafter.

Analysis of the transient absorption dynamics on the sub-ps time scale in SCy6803

A Gaussian-shaped instrument response function (IRF) of ≈133 fs FWHM is used, with parameters μ for the time of the IRF maximum and Δ for the FWHM of the IRF. The wavelength dependence of the parameter μ is described by a first order polynomial in the wavenumber domain. A "coherent artefact" (CA) straddling time zero is present in the transient absorption of Figure 2 and Figure S 1. This is modelled with a term $IRF(\mu,\Delta)\cdot IRFAS$. It contains a matrix $IRF(\mu,\Delta)$ with the zeroth, first and second derivative of the IRF [1,2], cf. Figure S 4A. The IRFAS amplitudes associated with each IRF derivative are wavelength dependent, cf. Figure S 4B,C. The first IRFAS (black) show large amplitudes straddling the excitation wavelength of 670 (Figure S 4B) and 700 nm (Figure S 4C). In addition, with 670 nm excitation a damped oscillation[2] (Figure S 4D) is present, with a frequency of ≈450 cm^{-1} and decaying with a rate of ≈7.7 ps^{-1}.

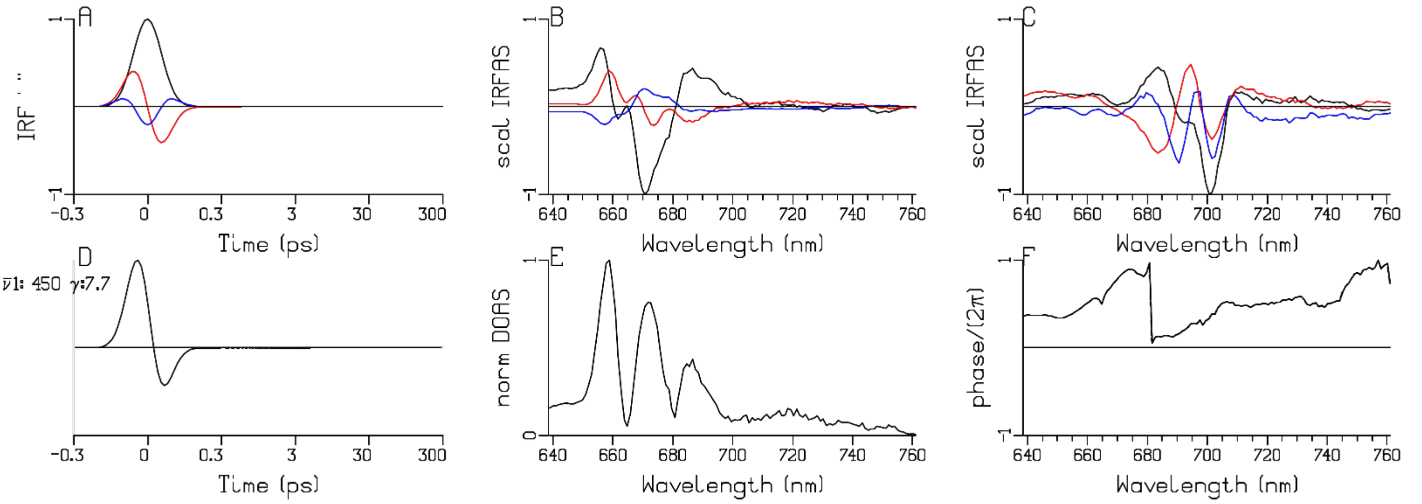

Figure S 4. Overview of the analysis of the sub-ps dynamics in reduced PSI complex of SCy6803 (related to Figure 3). (A) zeroth, first and second derivative of the IRF with 670 nm excitation (black, red and blue, respectively). (B) scaled IRFAS. Scaling of the IRFAS is such that the product of the IRFAS and the IRF derivative is the contribution to the fit. Thus, the black IRFAS has the largest contribution to the fit. Note that the time axis in (A,D) is linear until 0.3 ps and logarithmic thereafter.

Amplitude matrices of WL-PSI in SCy6803

A species\τ (ps)	0.37	0.54	1.78	6.36	14.8	22.6	long lived	input
Ant1	0.852	0.011	0.008	0.003	0.002	0.005	0	0.88
Bulk Chl a	-1.080	0.189	0.385	0.177	0.113	0.325	0	0.11
Red Chl a2	0.014	-0.004	-0.029	-0.180	0.065	0.133	0	0
WL-RC	0.223	-0.344	0.061	0.020	0.007	0.042	0	0.01
RP1	-0.077	0.172	-0.110	-0.197	-1.715	1.927	0	0
RP2	0.002	-0.005	0.011	0.073	1.483	-2.554	0.990	0
Red Chl a1	0.066	-0.018	-0.326	0.103	0.047	0.128	0	0
sum	0	0	0	0	0.003	0.007	0.990	1

B species\τ (ps)	0.37	0.54	1.78	6.36	14.8	22.6	long lived	input
Ant1	-0.002	-0.005	-0.001	0.000	0.002	0.006	0	0
Bulk Chl a	0.003	-0.085	-0.036	-0.018	0.131	0.345	0	0.34
Red Chl a2	0.000	0.002	0.003	0.019	0.076	0.142	0	0.24
WL-RC	-0.001	0.155	-0.006	-0.002	0.008	0.045	0	0.20
RP1	0.000	-0.077	0.010	0.021	-2.001	2.048	0	0
RP2	0.000	0.002	-0.001	-0.008	1.731	-2.714	0.990	0
Red Chl a1	0.000	0.008	0.030	-0.011	0.055	0.136	0	0.22
sum	0	0	0	0	0.003	0.007	0.990	1

Table S 1. Amplitude matrix of the reduced PSI complex of WT SCy6803 after 670 (A) or 700 (B) nm excitation (related to Figure 4). Key: Ant1 (light green), Bulk Chl a (dark green), Red Chl a1 (orange), Red Chl a2 (red), WL-RC (black), RP1 (cyan) and RP2 (blue).

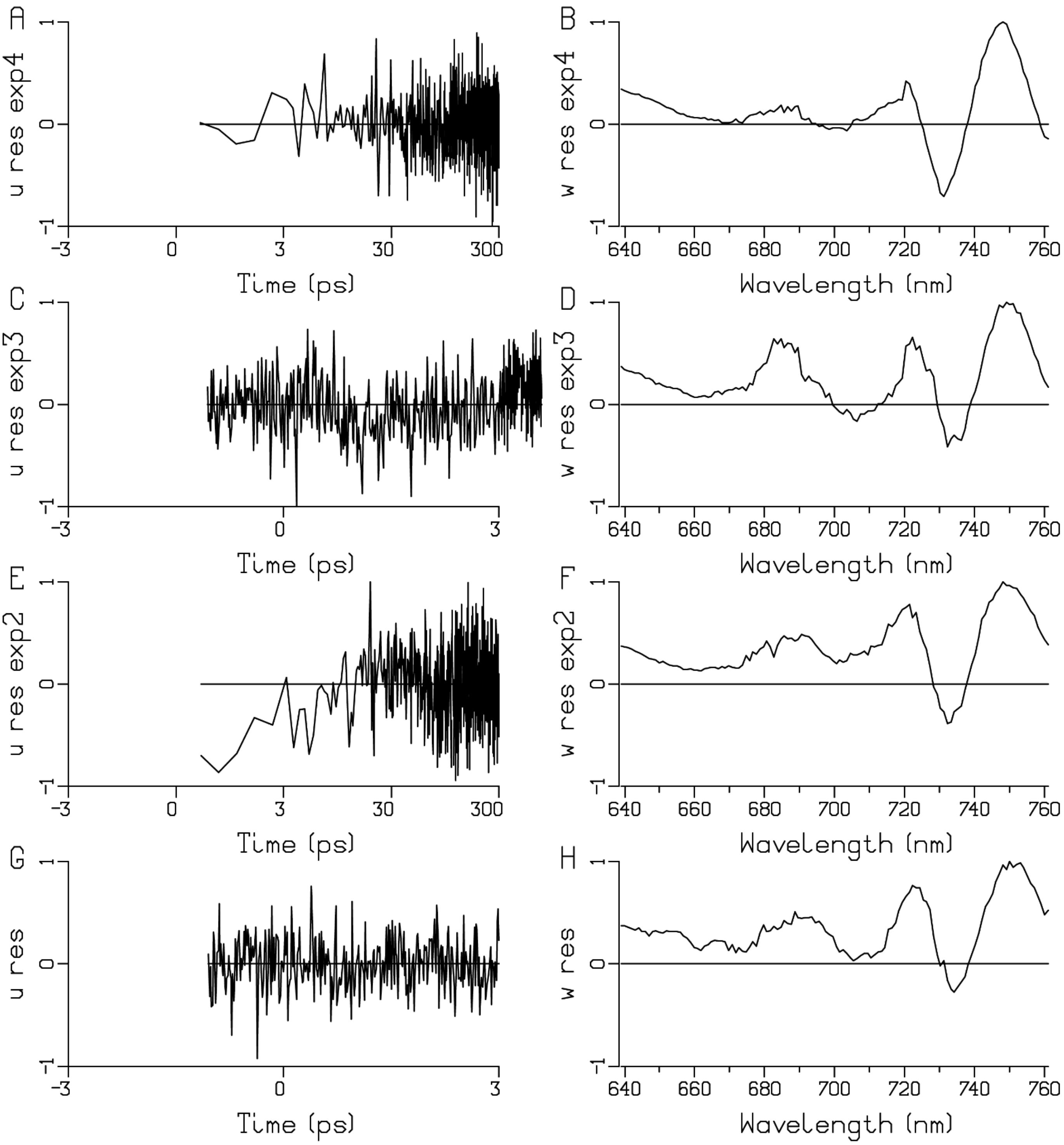

Figure S 5. First left (A,C,E,G) and right (B,D,F,H) singular vectors resulting from the singular value decomposition (SVD) of the residual matrix of WL-PSI of WT Synechocystis PCC6803 resulting from a *target* analysis using the kinetic scheme of Figure 4A (related to Figure 4). Note that all first left singular vector panels (A,C,E,G) show no trends at all. Key A,B: WL 700 nm excitation TimeRange(TR)2; C,D: WL 700 nm excitation TR1; E,F: WL 670 nm excitation TR2; G,H: WL 670 nm excitation TR1. Note that the time axis in (A,C,E,G) is linear until 3 ps and logarithmic thereafter.

Spectral fits of the SAS of SCo7335

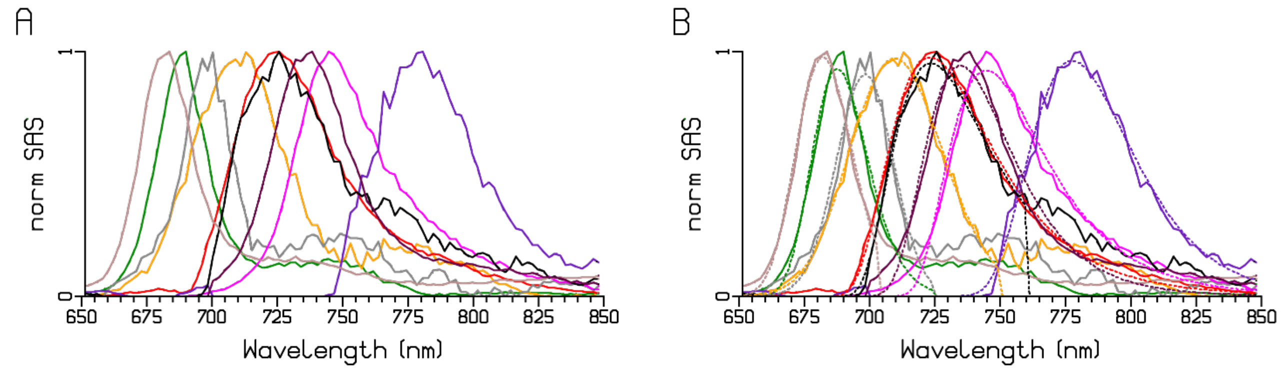

Figure S 6. Normalized SAS of SCo7335 (A) with superimposed spectral fits (dotted lines) using skewed Gaussian shapes (B) (related to Figure 6). Key: Bulk Chl a (dark green), Red Chl a1 (orange), Red Chl a2 (red), WL-RC (grey), FRL-RC (black), Chl f1 (magenta), Chl f2 (purple), free Chl a (brown) and free Chl f (maroon). Note that a single skewed Gaussian shape cannot well describe the vibrational tail of free Chl a, Bulk Chl a, or WL-RC.

Fit quality of the simultaneous target analysis of the emission of WL-PSI and FRL-PSI of CF9212

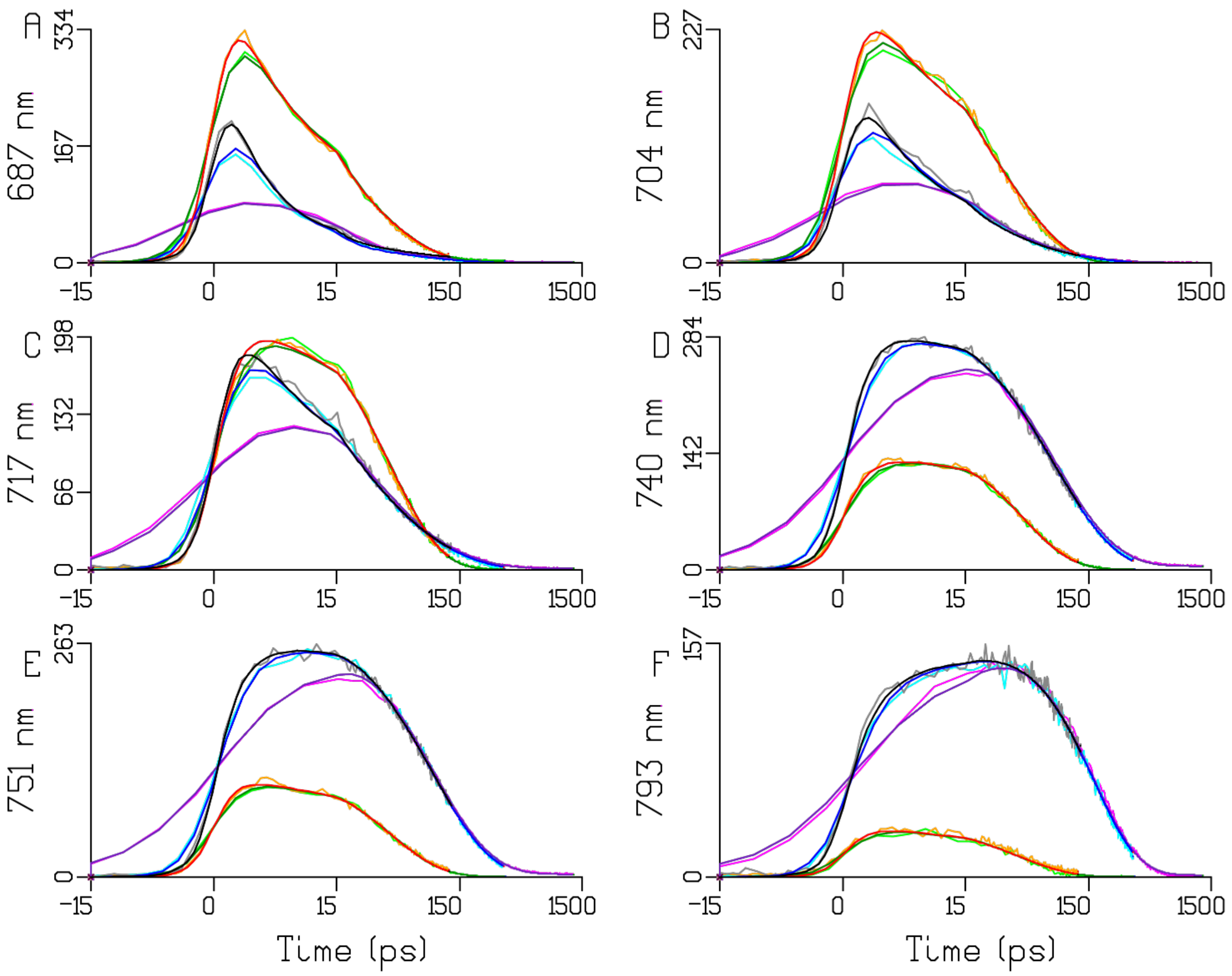

Figure S 7. Traces of data of WL-PSI (orange, green) and FRL-PSI (grey, cyan, magenta) and fit (WL-PSI: red, dark green; FRL-PSI: black, blue, purple) of CF9212 at selected detection wavelengths, written in the ordinate label (related to Figure 6). Note that the time axis is linear until 15 ps and logarithmic thereafter. Key: data measured with Time Range 1 (grey, orange), TR 2 (cyan, green) or TR4 (magenta). The FWHM of the IRF was 4.4, 6.3 and 18 ps with Time Range 1, 2 and 4, respectively. The overall rms error of the fit was 4.1.

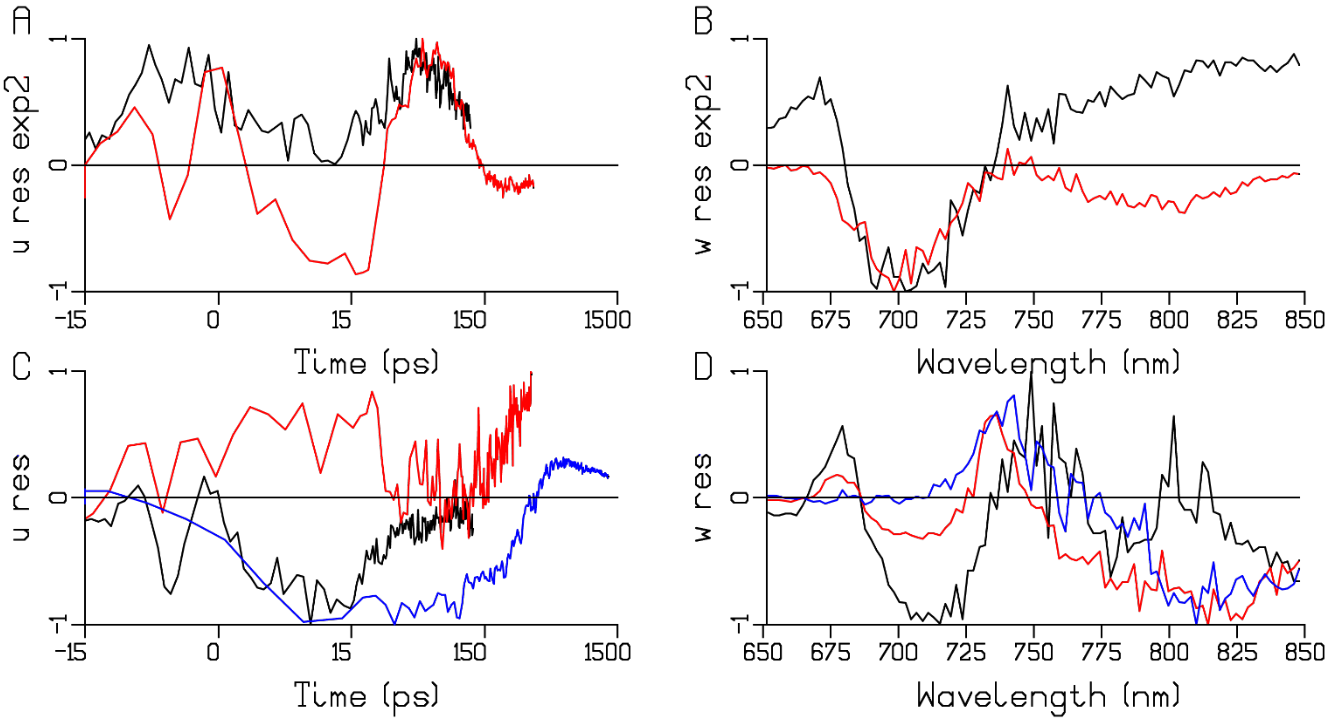

Figure S 8. First left (A,C) and right (B,D) singular vectors resulting from the singular value decomposition (SVD) of the residual matrix of WL-PSI (A,B) and FRL-PSI (C,D) of CF9212 resulting from a target analysis using the kinetic schemes of Figure 5B (related to Figure 6). Note that all panels show only small trends, which can be attributed to experimental variability, small differences in the wavelength calibration (especially with TR1), and long-term differences in the experimental setup, since the WL-PSI and FRL-PSI experiments have been performed with eight days in-between. Key: black, TR1; red, TR2; blue, TR4. Note that the time axis in (A,C) is linear until 15 ps and logarithmic thereafter.

Fit quality of the simultaneous target analysis of the emission of WL-PSI and FRL-PSI of FT7521

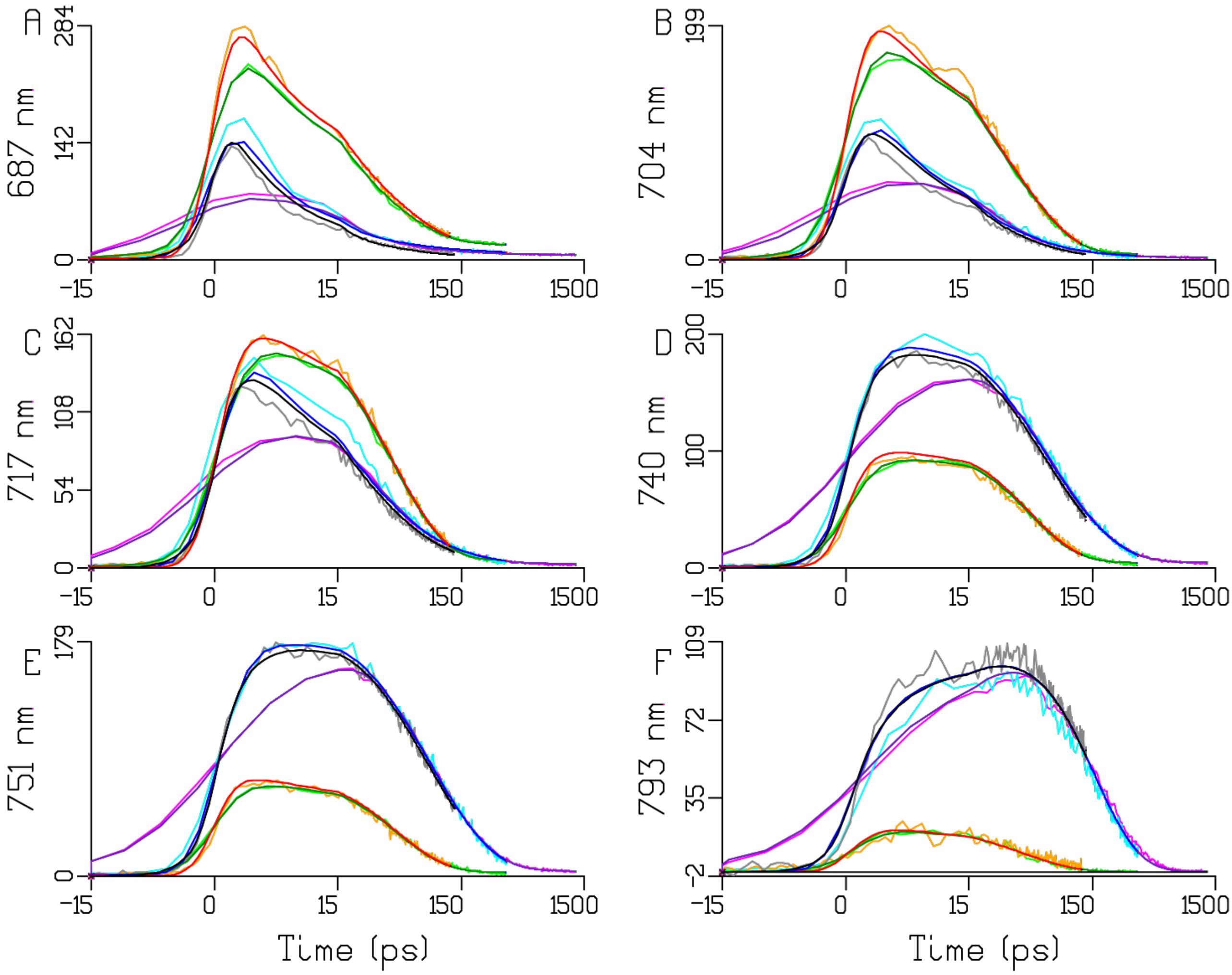

Figure S 9. Traces of data of WL-PSI (orange, green) and FRL-PSI (grey, cyan, magenta) and fit (WL-PSI: red, dark green; FRL-PSI: black, blue, purple) of FT7521 at selected detection wavelengths, written in the ordinate label (related to Figure 6). Note that the time axis is linear until 15 ps and logarithmic thereafter. Key: data measured with Time Range 1 (grey, orange), TR 2 (cyan, green) or TR4 (magenta). The FWHM of the IRF was 4.4, 6.3 and 18 ps with Time Range 1, 2 and 4, respectively. The overall rms error of the fit was 3.27.

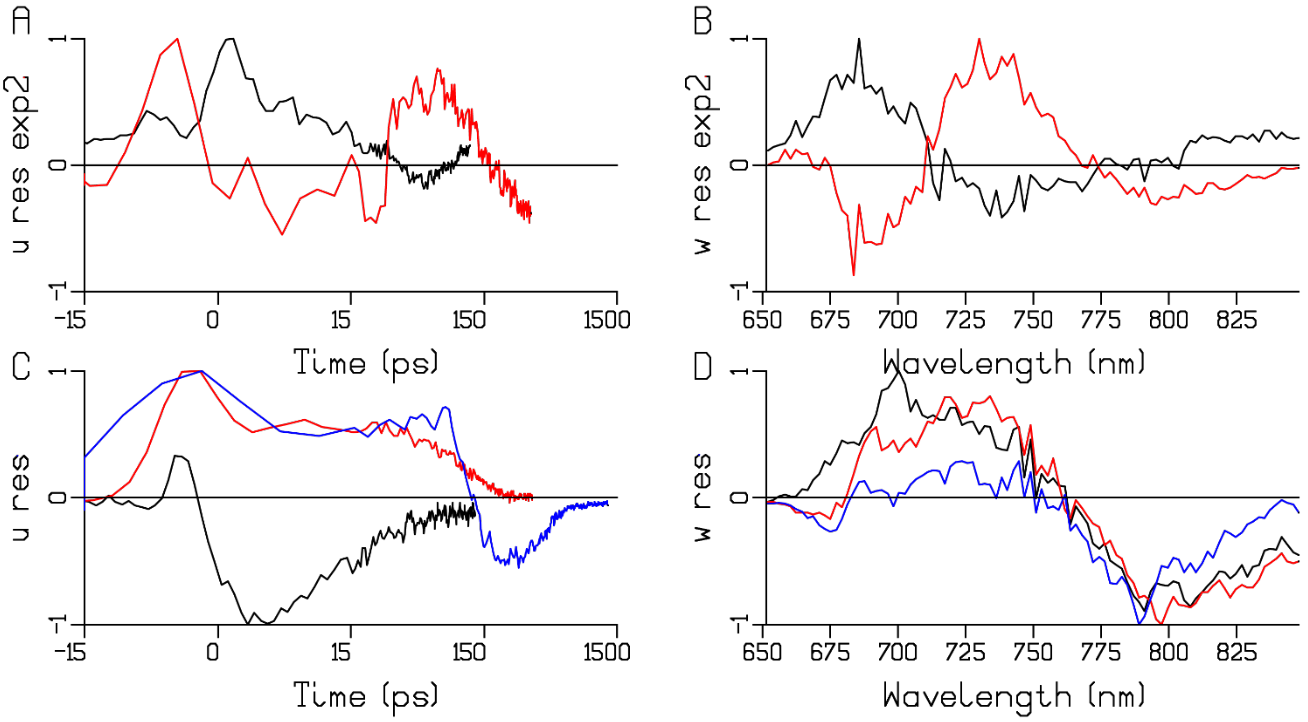

Figure S 10. First left (A,C) and right (B,D) singular vectors resulting from the singular value decomposition (SVD) of the residual matrix of WL-PSI (A,B) and FRL-PSI (C,D) of FT7521 resulting from a target analysis using the kinetic schemes of Figure 5 (related to Figure 6). Note that all panels show only small trends, which can be attributed to experimental variability, small differences in the wavelength calibration, and long-term differences in the experimental setup, since the WL-PSI and FRL-PSI experiments have been performed with eight days in-between. Key: black, TR1; red, TR2; blue, TR4. Note that the time axis in (A,C) is linear until 15 ps and logarithmic thereafter.

Amplitude matrices of WL-PSI and FRL-PSI in CT7203

A

species\τ (ps)	0.66	1.60	10.3	16.5	39	long lived	input
Bulk Chl a	0.014	0.337	0.243	0.000	0.253	0	0.848
Red Chl a1	-0.003	-0.292	0.197	0.000	0.163	0	0.065
Red Chl a2	0.000	-0.023	-0.246	-0.002	0.293	0	0.022
WL-RC	-0.028	0.050	0.020	0.000	0.024	0	0.065
WL-RP1	0.017	-0.079	-0.547	0.058	0.551	0	0
WL-RP2	-0.001	0.007	0.331	-0.056	-1.269	0.987	0
sum	0	0	0	0	0.014	0.987	1.000

B

species\τ (ps)	1.35	2.44	6.4	16.1	22	56	143	long lived	input
Bulk Chl a	0.478	0.002	0.235	0.001	0.020	0.013	0.013	0	0.761
Red Chl a1	-0.260	-0.005	0.296	0.001	0.015	0.009	0.009	0	0.065
Red Chl a2	-0.027	0.000	-0.087	-0.003	0.113	0.014	0.011	0	0.022
Chl f1	-0.083	-0.004	-0.230	-0.008	-0.111	0.307	0.194	0	0.065
Chl f2	-0.020	-0.010	-0.081	-0.015	-0.028	-0.313	0.489	0	0.022
FRL-RC	-0.155	0.098	0.057	0.020	0.013	0.004	0.029	0	0.065
FRL-RP1	0.073	-0.095	-0.309	0.154	0.069	0.014	0.094	0	0
FRL-RP2	-0.006	0.014	0.119	-0.149	-0.090	-0.047	-0.807	0.965	0
sum	0	0	0	0	0	0.001	0.033	0.965	1.000

Table S 2. Amplitude matrix of PS I complexes of WL-PSI (A) and FRL-PSI (B) of CT7203 at RT after 400 nm excitation (related to Figure 5). Key: Bulk Chl a (dark green), Red Chl a1 (orange), Red Chl a2 (red), WL-RC (grey), WL-RP1 (cyan), WL-RP2 (blue), Chl f1 (magenta), Chl f2 (purple), FRL-RC (black), FRL-RP1 (brown), and FRL-RP2 (maroon).

Global analysis of the transient absorption dynamics of WL-PSI and FRL-PSI of FT7521

First, the global analysis of the transient absorption dynamics of WL-PSI of FT7521 [3] and SCy6803 reduced will be compared. Disregarding the sub-ps component (cf. Figure 3), the EADS and lifetimes of WL-PSI of FT7521 and SCy6803 reduced are collated in Figure S 11 and Table S 3. The global analysis results of WL-PSI of FT7521 (Figure S 11A,B) are very different from SCy6803 reduced (Figure S 11C,D). In particular, with 720 nm excitation (Figure S 11B) the FT7521 long lived EADS around 705 nm (purple) is much smaller than the dark green EADS (41 ps), in contrast to reduced SCy6803 (Figure S 11C,D) where the amplitude around 705 nm of the long lived EADS is only a bit smaller. This large drop in amplitude is attributed to the quenching of a large part of the excited states by an oxidized FT7521 WL-RC. Second, the global analysis of the transient absorption dynamics of FRL-PSI of FT7521 [3] and the emission will be compared. Disregarding again the sub-ps component, the EADS and lifetimes are collated in Figure S 12 and Table S 4. Note the correspondence of the spectral evolution in Figure S 12A,B, where the EAS are mirrored by the first four EADS. Information about the radical pairs is of course lacking from the EAS. Analogously to Figure S 11B, the long-lived EADS (purple in Figure S 12B-D) are relatively small compared to the first EADS. Thus, we can conclude that the TA data of FT7521 [3] must be modeled in the target analysis as a mixture of reduced and photo-oxidized PSI complexes. Therefore, the RP2 quantum yield (QY) of WL-PSI in Figure 7B is ≈50% (cf. Table S 8) and the RP2 QY of FRL-PSI in Figure 7G is ≈31% (cf. Table S 9). In our target analysis the oxidized RC compartment acts like a sink that quenches the excitations transferred to it. The net result of the quenched excitation does not result in a spectral change since the oxidized RC remains unchanged. Thus, the oxidized RC compartment has a zero SADS.

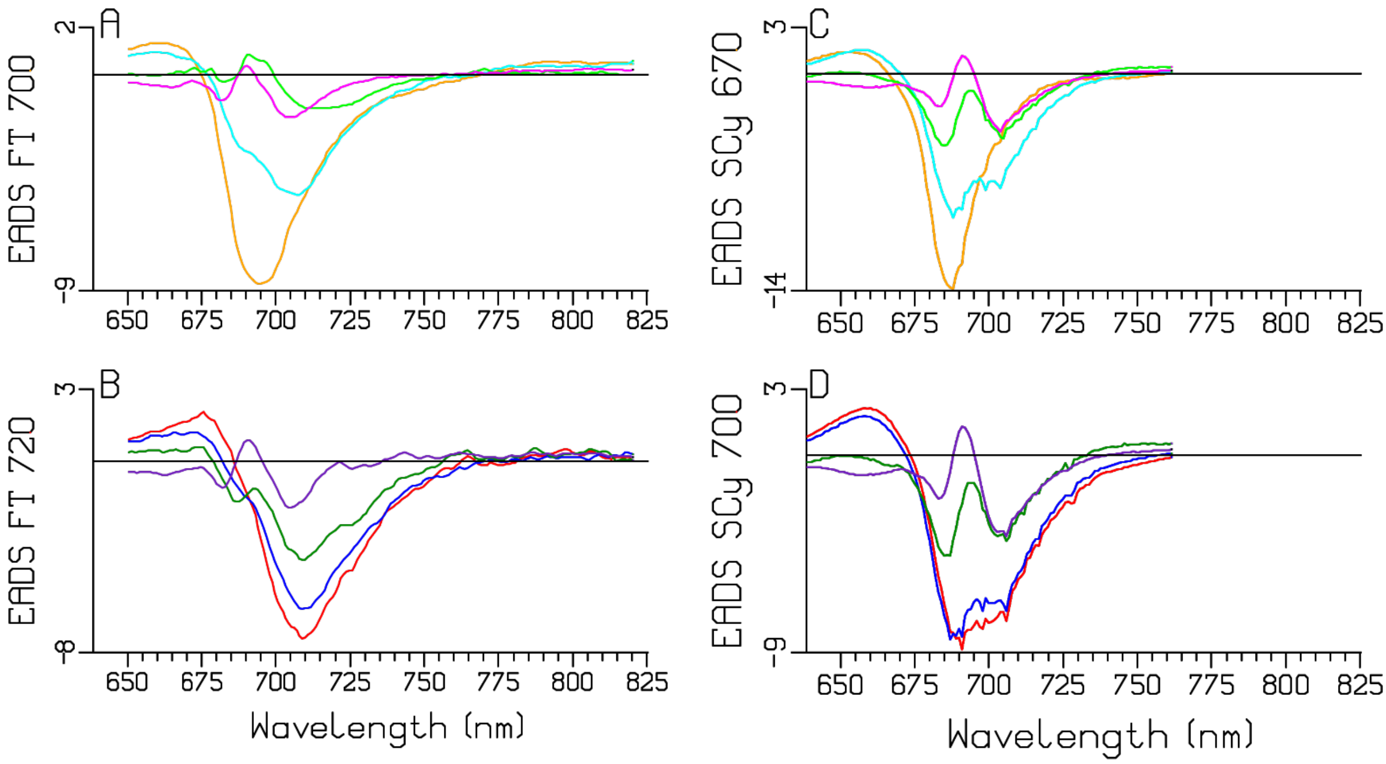

Figure S 11. Evolution Associated Difference Spectra (EADS) of WL-PSI of FT7521 (A,B) and SCy6803 reduced (C,D) (related to Figure 7). The excitation wavelength is written in the ordinate label. Lifetimes are collated in Table S 3.

	sample	λexcitation	condition	τ1	τ2	τ3	τ4
A	FT7521	700	ox/red	2.0	24	40	long lived
B	FT7521	720	ox/red	1.3	12	41	long lived
C	SCy6803	670	reduced	2.6	16	26	long lived
D	SCy6803	700	reduced	1.0	17	26	long lived

Table S 3. Lifetimes and experimental conditions of the EADS in Figure S 11 (related to Figure 7).

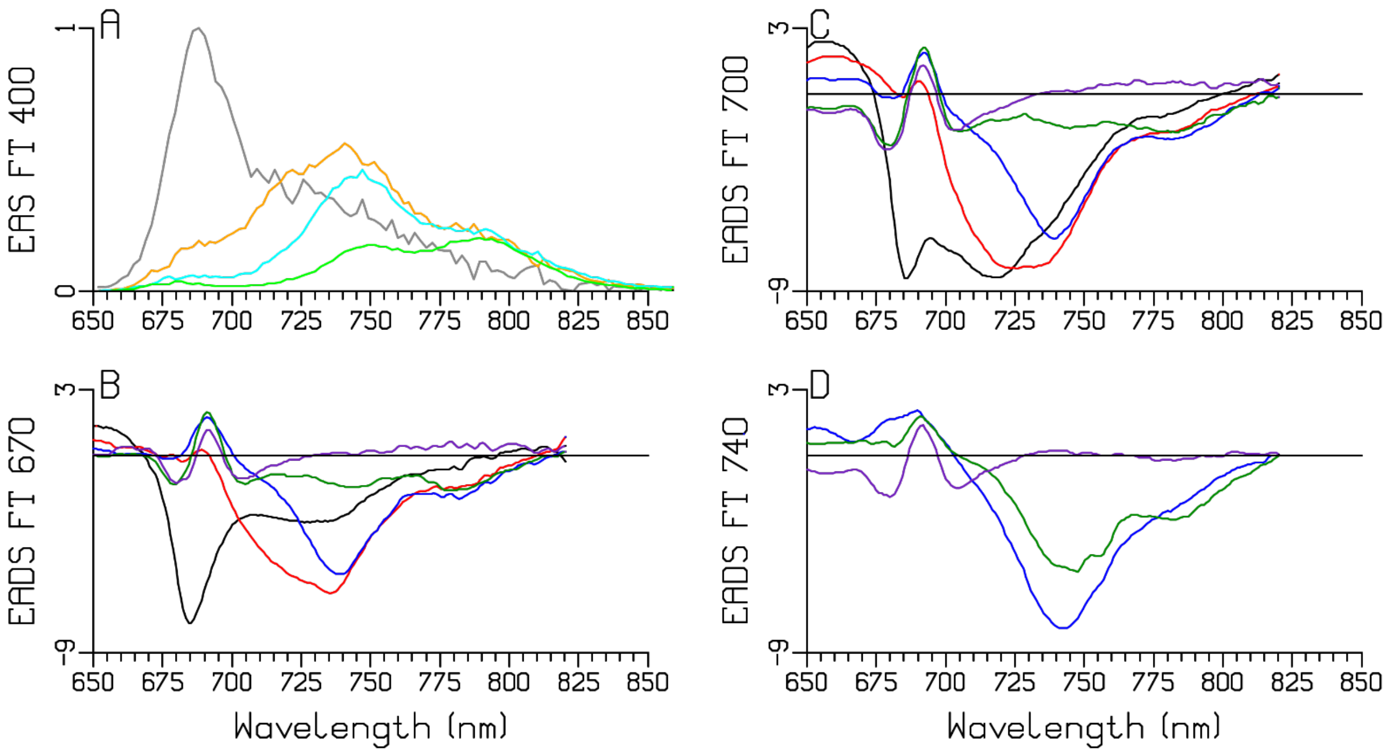

Figure S 12. Evolution Associated Spectra (EAS) (A) and Evolution Associated Difference Spectra (EADS) (B,C,D) of FRL-PSI of FT7521 (related to Figure 7). The excitation wavelength is written in the ordinate label. Lifetimes are collated in Table S 4.

	sample	λexcitation	condition	τ1	τ2	τ3	τ4	τ5
A	FT7521	400	reduced	3.5	14	51	120	long lived
B	FT7521	670	ox/red	3.0	17	60	230	long lived
C	FT7521	700	ox/red	3.0	17	62	289	long lived
D	FT7521	740	ox/red			24	164	long lived

Table S 4. Lifetimes and experimental conditions of the EAS and EADS in Figure S 12 (related to Figure 7).

Fit quality of the simultaneous target analysis of the transient absorption of WL-PSI and FRL-PSI of FT7521

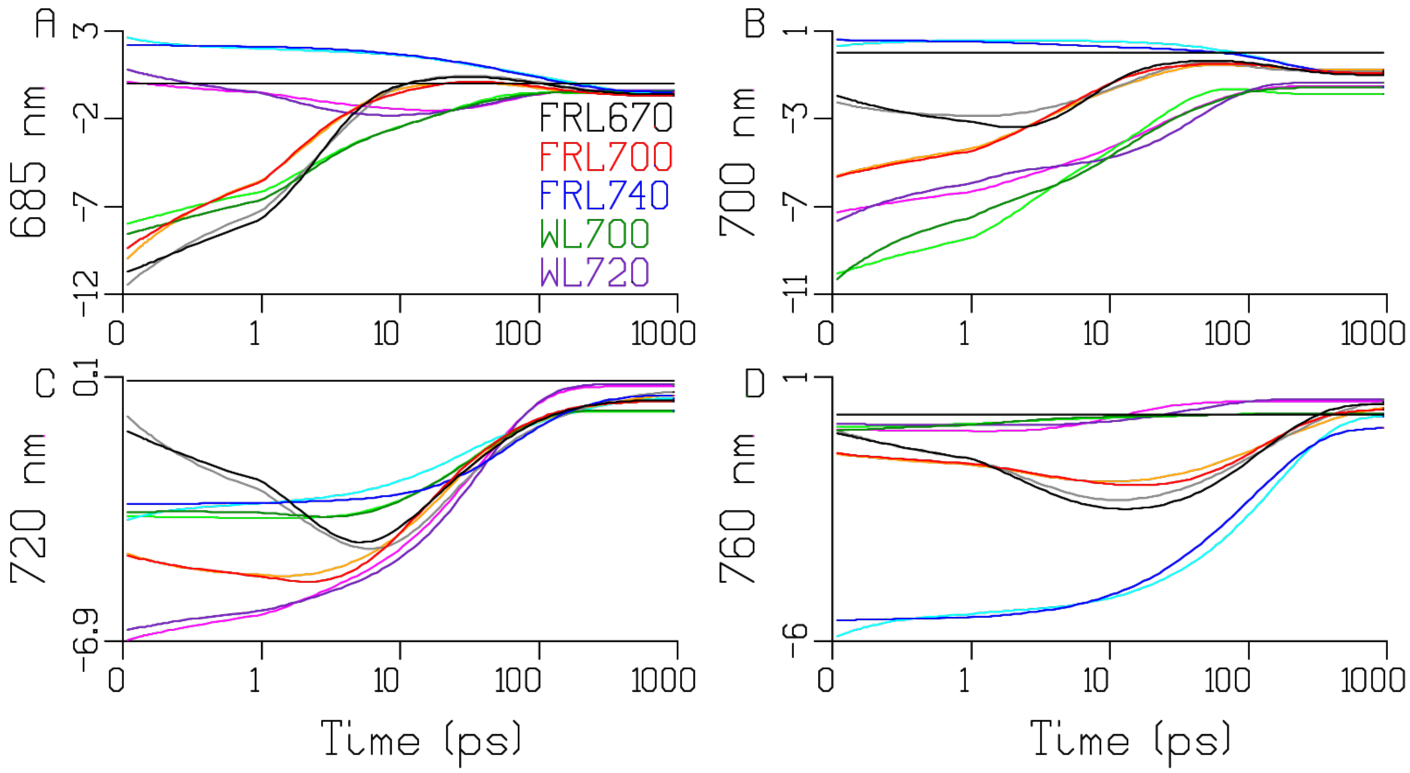

Figure S 13. Transient absorption (in units of mOD) of WL-PSI and FRL-PSI of FT7521 at four selected wavelengths (indicated in the ordinate label) (related to Figure 7). Key excitation wavelengths: FRL 670 nm (grey), FRL 700 nm (orange), FRL 740 nm (cyan), WL 700 nm (green) and WL 720 nm (magenta). Black, red, blue, dark green and purple lines indicate the simultaneous target analysis fit. Note that the time axis is linear until 1 ps and logarithmic thereafter. Note also that each panel is scaled to its maximum. The overall rms error of the fit was 0.16 mOD.

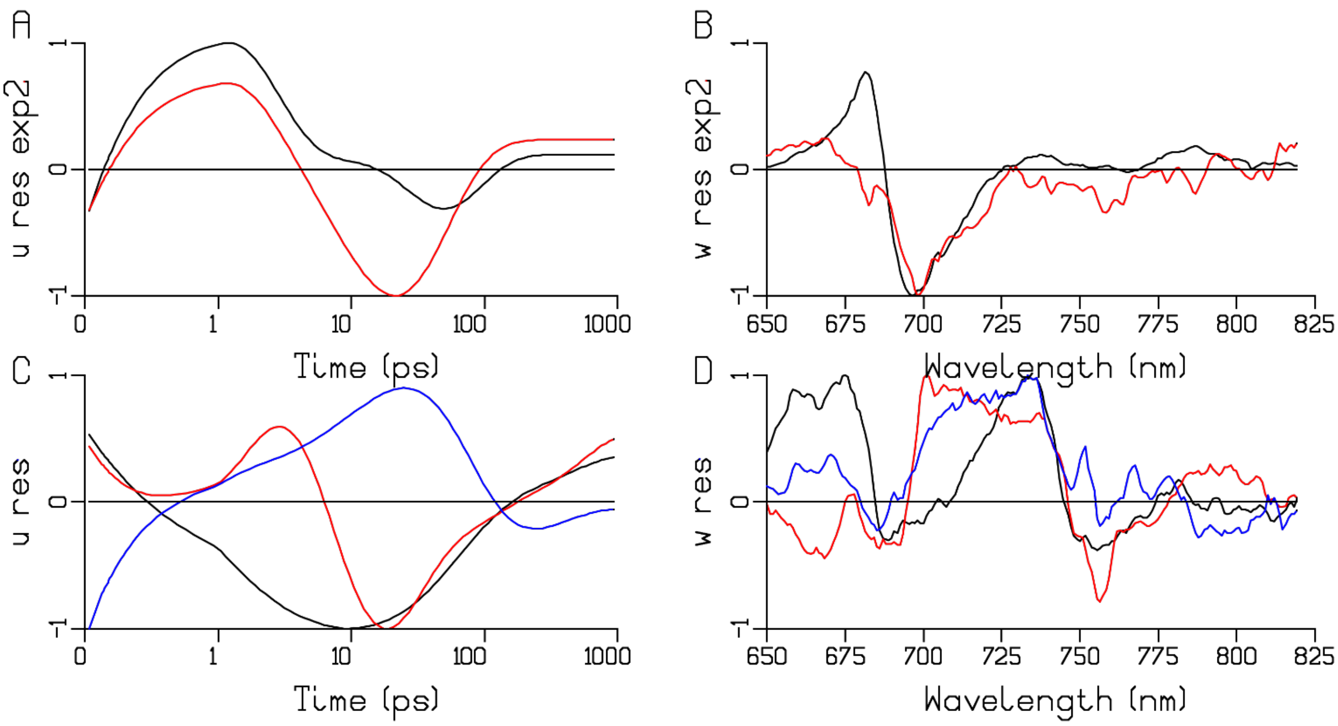

Figure S 14. First left (A,C) and right (B,D) singular vectors resulting from the singular value decomposition (SVD) of the residual matrix of WL-PSI (A,B) and FRL-PSI (C,D) of FT7521 resulting from a target analysis using the kinetic schemes of Figure 7A,F (related to Figure 7). Key A,B: black, WL 700 nm excitation; red, 720; C,D: black, FRL 670 nm excitation; red, 700; blue, 740. Note that the time axis in (A,C) is linear until 1 ps and logarithmic thereafter.

Alternative target analysis of the transient absorption of WL-PSI and FRL-PSI of FT7521

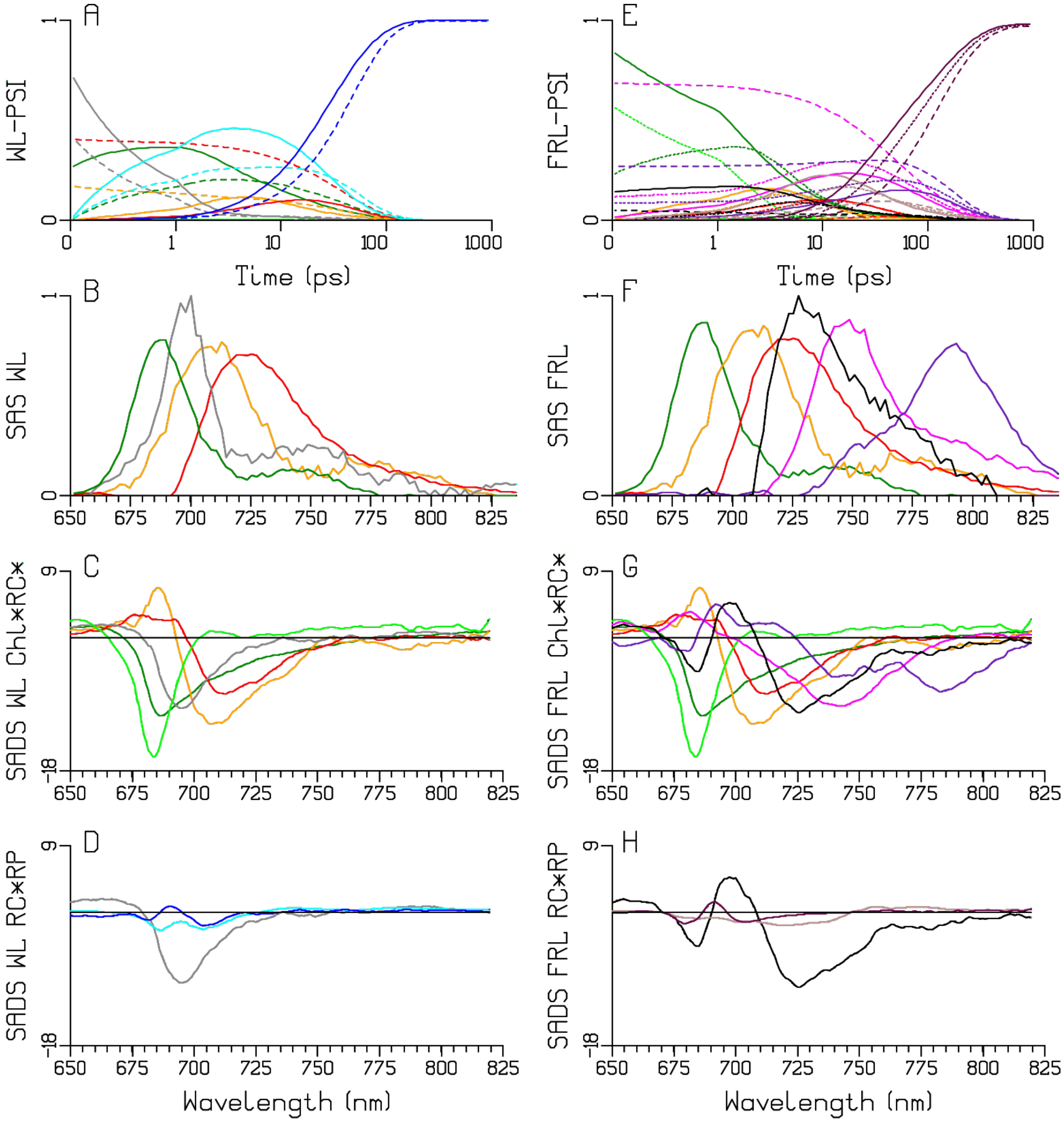

Figure S 15. Alternative target analysis of the transient absorption of WL-PSI and FRL-PSI of FT7521 at 6°C without photo-oxidized PSI complexes (i.e. near unity quantum yield) using the kinetic schemes of Figure 7A,F (related to Figure 7). Key: Ant1 (light green), Bulk Chl a (dark green), Red Chl a1 (orange), Red Chl a2 (red), WL-RC (grey), FRL-RC (black), Chl f1 (magenta), Chl f2 (purple), WL-RP1 (cyan), WL-RP2 (blue), FRL-RP1 (brown), and FRL-RP2 (maroon). Estimated populations and SADS (in mOD) of WL-PSI (A, solid 700, dashed 720 nm excitation) and FRL-PSI (E, solid 700, dashed 740, dotted 670 nm excitation) of FT7521. Note that the time axis is linear until 1 ps and logarithmic thereafter. SADS of the excited states and of RP1 and RP2 (C,D,G,H). The SAS from Figure 6F have been redrawn in (B,F) for comparison. The rms error of the fit was 4% larger than in the analysis with the photo-oxidized PSI complexes.

Thermodynamic considerations

The estimated SAS (Figure 6B,D,F,H, and Table 3) exhibit smooth bands with maxima at ≈689 nm (Bulk Chl a), ≈699 nm (WL-RC, grey), ≈726-731 nm (FRL-RC, black), ≈711 nm (Red Chl a1), ≈725 nm (Red Chl a2), ≈746-755 nm (Chl f1) and ≈780-797 nm (Chl f2). The SAS can be approximated with skewed Gaussian shapes [4] thereby estimating the wavenumber of maximum emission $\overline{\nu}_{\max}$, cf. Figure S 6B. Thus, we find the $\overline{\nu}_{\max}$ collated in Table S 5A (in cm^{-1}), and when converted to k_BT, Table S 5C.

A

1/cm	Bulk Chl a	Red Chl a1	Red Chl a2	WL-RC	FRL-RC	Chl f1	Chl f2
SCo7335	14533	14054	13781	14311	13777	13390	12821
CF9212	14505	14061	13760	14315	13742	13403	12553
FT7521	14538	14082	13808	14305	13683	13376	12574
CT7203	14502	14046	13867	14303	13708	13248	12579

B

nm	Bulk Chl a	Red Chl a1	Red Chl a2	WL-RC	FRL-RC	Chl f1	Chl f2
SCo7335	688	712	726	699	726	747	780
CF9212	689	711	727	699	728	746	797
FT7521	688	710	724	699	731	748	795
CT7203	690	712	721	699	730	755	795

C

kB.T	Bulk Chl a	Red Chl a1	Red Chl a2	WL-RC	FRL-RC	Chl f1	Chl f2
SCo7335	71.4	69.0	67.7	70.3	67.6	65.7	63.0
CF9212	71.2	69.0	67.6	70.3	67.5	65.8	61.6
FT7521	71.4	69.1	67.8	70.2	67.2	65.7	61.7
CT7203	71.2	69.0	68.1	70.2	67.3	65.1	61.8

D

kB.T	Bulk Chl a	Red Chl a1	Red Chl a2	WL-RC	FRL-RC	Chl f1	Chl f2
SCo7335	0	-2.4	-3.7	-1.1	-3.7	-5.6	-8.4
CF9212	0	-2.2	-3.7	-0.9	-3.7	-5.4	-9.6
FT7521	0	-2.2	-3.6	-1.1	-4.2	-5.7	-9.6
CT7203	0	-2.2	-3.1	-1.0	-3.9	-6.2	-9.4

Table S 5. Location of the maximum emission $\overline{\nu}_{\max}$ in cm^{-1} (A) in k_BT (C, 1 k_BT=207 cm^{-1}) or $\lambda_{\max}$ in nm (B) estimated from the SAS in Figure 6 (related to Figure 6). In (D) the difference relative to Bulk Chl a from (C).

The Gibbs free energy relative to that of the Bulk Chl a which is estimated from the data (and computed from the kinetic schemes of Figure 5) is collated in Table S 6A. Analogously, the enthalpy relative to that of the Bulk Chl a is collated in Table S 5D and copied to Table S 6B. The difference ΔH−ΔG=TΔS is computed and shown in Table S 6C. Note that the enthalpy advantage of the Red Chl a compartments relative to the Bulk Chl a (Table S 6B) is smaller than the entropy advantage of the Bulk Chl a compartment (Table S 6C), explaining the positive Gibbs free energy relative to that of the Bulk Chl a (Table S 6A). Finally, the number of pigments "N" is computed from the entropy difference ($N = N_{Bulk} \exp(\Delta S / k_B)$) and shown in Table S 6D.

A

ΔG	Bulk Chl a	Red Chl a1	Red Chl a2	WL-RC
SCo7335	0	1.11	0.66	1.50
CF9212	0	1.28	0.16	1.50
FT7521	0	0.82	0.19	1.50
CT7203	0	0.51	0.42	1.50

Bulk Chl a	Red Chl a1	Red Chl a2	FRL-RC	Chl f1	Chl f2
0	1.00	0.55	-1.65	-2.73	-1.98
0	1.17	0.06	-1.75	-2.17	-2.78
0	0.71	0.08	-1.75	-2.05	-2.60
0	0.40	0.31	-1.75	-2.44	-3.28

B

ΔH	Bulk Chl a	Red Chl a1	Red Chl a2	WL-RC
SCo7335	0	-2.4	-3.7	-1.1
CF9212	0	-2.2	-3.7	-0.9
FT7521	0	-2.2	-3.6	-1.1
CT7203	0	-2.2	-3.1	-1.0

Bulk Chl a	Red Chl a1	Red Chl a2	FRL-RC	Chl f1	Chl f2
0	-2.4	-3.7	-3.7	-5.6	-8.4
0	-2.2	-3.7	-3.7	-5.4	-9.6
0	-2.2	-3.6	-4.2	-5.7	-9.6
0	-2.2	-3.1	-3.9	-6.2	-9.4

C

ΔH-ΔG=TΔS	Bulk Chl a	Red Chl a1	Red Chl a2	WL-RC
SCo7335	0	-3.5	-4.3	-2.6
CF9212	0	-3.5	-3.8	-2.4
FT7521	0	-3.1	-3.8	-2.6
CT7203	0	-2.8	-3.5	-2.5

Bulk Chl a	Red Chl a1	Red Chl a2	FRL-RC	Chl f1	Chl f2
0	-3.4	-4.2	-2.1	-2.9	-6.4
0	-3.4	-3.7	-2.0	-3.2	-6.8
0	-3.0	-3.7	-2.4	-3.7	-7.0
0	-2.6	-3.4	-2.1	-3.7	-6.2

D

"N"	Bulk Chl a	Red Chl a1	Red Chl a2	RC WL
SCo7335	78	2.4	1.0	5.9
CF9212	78	2.4	1.7	6.8
FT7521	78	3.7	1.8	5.5
CT7203	78	5.0	2.3	6.6

Bulk Chl a	Red Chl a1	Red Chl a2	RC FRL	Chl f1	Chl f2
70	2.4	1.0	8.9	3.9	0.11
70	2.4	1.7	9.5	2.7	0.08
70	3.7	1.8	6.1	1.8	0.06
70	5.0	2.3	8.2	1.7	0.15

Table S 6. Thermodynamic quantities of WL-PSI (left) and FRL-PSI (right) relative to Bulk Chl a in k_BT (1 k_BT=207 cm^{-1}), ΔG computed from Figure 5, ΔH copied from Table S 5D (related to Figure 6).

Analogous computations based upon the estimated SADS for the location of the extremum of the bleach plus stimulated emission (Figure 7D,I and Figure 4C) are collated in Table 1 and Table S 7. The entropy of the Bulk Chl a compartment is larger than that of all other compartments, in accordance with the number of Bulk Chl a pigments being many times larger than the number of pigments in any of the other compartments. Precise quantification of the number of pigments in each compartment is difficult, since it crucially depends on the validity of the many assumptions that have been used in the target analysis. Also, in view of the excitonic interactions involved in many of the compartments, the numbers in Table 1, Table S 6D and Table S 7 should be interpreted cautiously. Nevertheless, the WL-PSI "N" of Table 1, Table S 6D and the FRL-PSI "N" of Table S 7 are very reasonable. The small "N" value with Chl f2 in Table S 6D can be attributed to the very low ΔH, which in emission is more than two k_BT lower than in transient absorption. In the steady state absorption the Chl f2 maximum was at 771 nm [5]. The steady state emission was at 789 nm [5], which indicates a large Stokes' shift of ≈18 nm. Based upon the numbers in Table S 5B and Table S 7 the Stokes' shift is even ≈26 nm. Thus, the unexpectedly small "N" value with Chl f2 in Table S 6D can be explained by its huge Stokes' shift. The "N" value of the Ant1 compartment that contains the Chl a pigments absorbing to the blue of the Bulk Chl a (light vs. dark green in Figure 7) and is selectively excited by the 670 nm pump pulse is about 2 (Table 1, Table S 7).

A	Ant1	Bulk Chl a	Red Chl a1	Red Chl a2	WL-RC
λ max (nm)	684	689	705	715	695
ν max (1/cm)	14612	14509	14194	13979	14387
ν max (kB.T)	75.3	74.8	73.2	72.1	74.2
ΔH (kB.T)	0.5		-1.6	-2.7	-0.6
ΔG (kB.T)	4.1		0.7	0.1	1.4
ΔH-ΔG=TΔS (kB.T)	-3.6		-2.3	-2.8	-2.0
"N"	2.2	78	7.7	4.7	10.5

B	Ant1	Bulk Chl a	Red Chl a1	Red Chl a2	FRL-RC	Chl f1	Chl f2
λ max (nm)	684	689	705	715	728	745	769
ν max (1/cm)	14612	14509	14194	13979	13735	13431	13007
ν max (kB.T)	75.3	74.8	73.2	72.1	70.8	69.3	67.1
ΔH (kB.T)	0.5		-1.6	-2.7	-4.0	-5.6	-7.7
ΔG (kB.T)	4.0		0.6	0.0	-1.9	-2.2	-2.8
ΔH-ΔG=TΔS (kB.T)	-3.5		-2.2	-2.7	-2.1	-3.4	-5.0
"N"	2.2	70	7.7	4.7	8.4	2.4	0.5

Table S 7. Thermodynamic properties of the WL-PSI (A) and FRL-PSI (B) estimated from the SADS of FT7521 related to Figure 7. Location of the extremum of the bleach plus stimulated emission in Figure 7D,I: $\lambda_{\max}$ in nm, $\bar{\nu}_{\max}$ in cm^{-1} and in k_BT (1 k_BT=207 cm^{-1}). ΔH relative to Bulk Chl a in k_BT. ΔG taken from Figure 7A,F. ΔH-ΔG=TΔS (kB.T) and "N" computed via $N = N_{Bulk}\exp(\Delta S / k_B)$.

Amplitude matrices of WL-PSI and FRL-PSI in FT7521 after FRL excitation

With FR light the redmost absorbing compartments will be selectively excited. It is estimated that in WL-PSI the 720 nm excitation light is absorbed by Red Chl a1 (17%), Red Chl a2 (40%), and WL-RC (43%). Note that the amplitude matrices here only apply for the reduced PSI complexes. From the computed amplitude matrix (Table S 8) the RP1 populations starts to rise in 0.66 ps (because of the assumed 43% direct excitation of the WL-RC). The final decay of RP1 is with 40 ps, which is also the dominant lifetime of the equilibrated excited states, and the trapping time observed in the emission. The yield of RP2 is (0.488/0.492=) 99%.

species\τ (ps)	0.66	1.37	1.7	8.8	17	40	long lived	input
Bulk Chl a	-0.103	0.006	-0.013	-0.003	0.000	0.113	0	0
Red Chl a1	0.017	-0.003	0.012	-0.002	0.000	0.060	0	0.084
Red Chl a2	0.004	0.000	0.001	0.003	0.006	0.185	0	0.198
WL-RC	0.200	0.001	-0.002	0.000	-0.001	0.012	0	0.210
WL-RP1	-0.124	-0.001	0.004	0.005	-0.163	0.280	0	0
Ant1	0.001	-0.002	-0.001	0.000	0.000	0.002	0	0
WL-RP2	0.005	0.000	0.000	-0.002	0.158	-0.649	0.488	0
sum	0	0	0	0	0	0.004	0.488	0.492

Table S 8. Amplitude matrix of the reduced WL-PSI complexes of FT7521 (related to Figure 7) after 720 nm excitation, selectively exciting Red Chl a1 (17%), Red Chl a2 (40%), and WL-RC (43%). Key: Bulk Chl a (dark green), Red Chl a1 (orange), Red Chl a2 (red), WL-RC (grey), WL-RP1 (cyan), and WL-RP2 (blue).

It is estimated that in FRL-PSI the 740 nm excitation light is absorbed by Chl f1 (68%), Chl f2 (27%) and FRL-RC (5%). From the computed amplitude matrix (Table S 9) the RP1 population starts to rise in 2.6 ps (because of the estimated 5% direct excitation of the FRL-RC). Chl f1 equilibrates with Chl f2 in 43 ps. The final decays of RP1 are with 43 and 128 ps. The latter is also the dominant lifetime of the equilibrated excited states, and the trapping time observed in the emission. The yield of RP2 is (0.302/0.312=) 96.5%.

species\τ (ps)	1.39	1.72	2.6	6.6	17	24	43	128	long lived	input
Bulk Chl a	-0.002	-0.001	0.000	-0.005	0.000	-0.005	0.006	0.007	0	0
Red Chl a1	0.001	0.001	0.000	-0.005	0.000	-0.003	0.003	0.004	0	0
Red Chl a2	0.000	0.000	0.000	0.003	0.001	-0.023	0.011	0.008	0	0
Ant1	0.000	0.000	0.000	0.000	0.000	0.000	0.000	0.000	0	0
Chl f1	0.000	0.000	0.000	0.004	0.001	0.027	0.094	0.088	0	0.213
Chl f2	0.000	0.000	0.000	0.001	0.002	-0.001	-0.098	0.180	0	0.084
FRL-RC	0.001	0.001	0.008	-0.001	-0.005	-0.004	0.003	0.013	0	0.015
FRL-RP1	0.000	0.000	-0.008	0.008	-0.035	-0.019	0.011	0.044	0	0
FRL-RP2	0.000	0.000	0.001	-0.003	0.035	0.028	-0.029	-0.334	0.302	0
sum	0	0	0	0	0	0	0	0.010	0.302	0.312

Table S 9. Amplitude matrix of the reduced FRL-PSI complexes of FT7521 (related to Figure 7) after 740 nm excitation, selectively exciting Chl f1 (68%), Chl f2 (27%) and FRL-RC (5%). Key: Bulk Chl a (dark green), Red Chl a1 (orange), Red Chl a2 (red), FRL-RC (black), Chl f1 (magenta), Chl f2 (purple), FRL-RP1 (brown) and FRL-RP2 (maroon).

References

1. Kovalenko, S.A., Dobryakov, A.L., Ruthmann, J., and Ernsting, N.P. (1999). Femtosecond spectroscopy of condensed phases with chirped supercontinuum probing. Physical Review A *59*, 2369-2384. 10.1103/PhysRevA.59.2369.
2. van Stokkum, I.H.M., Kloz, M., Polli, D., Viola, D., Weißenborn, J., Peerbooms, E., Cerullo, G., and Kennis, J.T.M. (2021). Vibronic dynamics resolved by global and target analysis of ultrafast transient absorption spectra. The Journal of Chemical Physics *155*, 114113. 10.1063/5.0060672.
3. Cherepanov, D.A., Shelaev, I.V., Gostev, F.E., Aybush, A.V., Mamedov, M.D., Shen, G., Nadtochenko, V.A., Bryant, D.A., Semenov, A.Y., and Golbeck, J.H. (2020). Evidence that chlorophyll f functions solely as an antenna pigment in far-red-light photosystem I from Fischerella thermalis PCC 7521. Biochimica et Biophysica Acta (BBA) - Bioenergetics *1861*, 148184. https://doi.org/10.1016/j.bbabio.2020.148184.
4. van Stokkum, I.H.M., Larsen, D.S., and van Grondelle, R. (2004). Global and target analysis of time-resolved spectra. Biochimica Et Biophysica Acta *1657*, 82-104. 10.1016/j.bbabio.2004.04.011.
5. Tros, M., Mascoli, V., Shen, G., Ho, M.-Y., Bersanini, L., Gisriel, C.J., Bryant, D.A., and Croce, R. (2021). Breaking the Red Limit: Efficient Trapping of Long-Wavelength Excitations in Chlorophyll-f-Containing Photosystem I. Chem *7*, 155-173. https://doi.org/10.1016/j.chempr.2020.10.024.